Digest Journal of Nanomaterials and Biostructures

Dig. J. Nanomater. Bios. **2026**; 21(2): 55197
https://doi.org/10.31083/DJNB55197

Original Research

Influence of Al_2O_3 Content on the Structural Network and Thermal Stability of Lithium Borate Glasses

Mustafa K. Abid[1], Ali Q. Tuama[2,3,*]

[1]Department of Medical Physics, College of Science, Al-Karkh University of Science, 10011 Baghdad, Iraq
[2]Department of Renewable Energy, College of Energy & Environmental Sciences, Al-Karkh University of Science, 10011 Baghdad, Iraq
[3]School of Physics, Universiti Sains Malaysia (USM), 11800 Penang, Malaysia
*Correspondence: Aliq.tuama@kus.edu.iq (Ali Q. Tuama)

Academic Editor: Redouane Zitoune
Submitted: 6 January 2026 Revised: 13 March 2026 Accepted: 20 March 2026 Published: 23 June 2026

Abstract

The impact of Aluminum oxide (Al_2O_3) addition on thermal stability and structural networks present within lithium borate glass defined by the mixed composition of the simple ternary Li_2O–Al_2O_3–B_2O_3 system. This approach intends to separate the specific structure of Al_2O_3 contributions from any potential impacts of additional dopants or the complex chemistry of glasses studied previously. Glasses with variable amounts of Al_2O_3 were prepared through a standard melt-quench technique. Structural modifications were investigated using X-ray diffraction and Fourier transform infrared spectroscopy, with particular emphasis placed on the evolution of three-coordinated boron (BO_3) and four-coordinated boron (BO_4) units and the formation of four-coordinated aluminum (AlO_4) tetrahedra.Differential scanning calorimetry was used to evaluate thermal stability and both the glass transition temperature, crystallization temperature, and thermal stability window. Higher Al_2O_3 contents translated into enhanced network connectivity, more pronounced structural densification, and greater thermal stability. The results give an improved understanding of the structure-property relationship of this type of glass by illustrating the relationship between composition and properties. The findings support the use of the aluminate lithium borate glasses for applications requiring greater resistance to heat than what current materials can provide.

Keywords: lithium borate glasses; Al_2O_3; glass structure; thermal stability; network connectivity

1. Introduction

Borate-based glasses have been extensively studied and developed due to their low melting points, large compositional range, and unique structure derived from the presence of both trigonal three-coordinated boron (BO_3) and tetrahedral BO_4 units [1,2,3]. These attributes allow borate-based materials to be used in a number of different ways, such as in sealants, optics and thermally stable glass matrices [2]. The network connectivity, rigidity and thermal behaviour of the boron-oxygen units play a critical part in controlling the glass properties [3,4]. An important subset of borate glasses is lithium borate, where Li_2O is used as a network modifier. The addition of Li_2O converts some BO_3 units into tetrahedral BO_4, which increases the degree of polymerization of the glass network [4,5]. This structural change is often accompanied by increased rigidity, less free volume and greater thermal stability [6]. The BO_3/BO_4 ratio is often cited as an important structural parameter for determining the properties, both physical and thermal, of lithium borate glasses [5,7]. Aluminum oxide (Al_2O_3) has a functionally determined structural role in oxide glasses which can act as either a network former or an intermediate oxide [8]. Tetrahedrally coordinated Aluminum cations (Al^{3+}) are mainly included in borate-based oxide glasses containing sufficiently high concentration of compensating cations, forming four-coordinated aluminum (AlO_4) units [9]. The presence of AlO_4 tetrahedra in borate glasses increases the degree of connectivity, increases the density of the glass, and improves its thermal resistance to deformation [8]. In previous studies on both Aluminoborate and Lithium Aluminoborate oxide glasses containing aluminum, the addition of alumina increased the density of the glass, increased the glass transition temperature and crystallization temperature of the glass — demonstrating an increased strengthening influence of alumina upon the glass network [10,11]. Most of the previous studies thus far have been confined to studies involving complex or doped glasses and the influence of alumina in these types of systems has been mixed with the influence of other modifying agents or functional dopants [11]. As a result, the intrinsic structural and thermal role of Al_2O_3 is still insufficiently isolated from simple glass compositions and not systematically studied. Very few comprehensive studies have been performed to determine the fundamental role of Al_2O_3 when it is added to a ternary Li_2O–Al_2O_3–B_2O_3 system [11]. The present work attempts to bridge that information gap by establishing a systematic study to investigate how the content of Al_2O_3 affects the structural network and thermal stability of lithium borate glasses in a simple ternary composition. The effect of Al_2O_3 on network development and thermal properties can be assessed directly by keeping the amount of B_2O_3 constant (10–20 mol%) while varying

Al_2O_3 within this range. This guarantees there will be stable homogeneous glasses formed in the laboratory. X-ray diffraction (XRD), Fourier transform infrared spectroscopy (FTIR), density and molar volume measurements, and differential scanning calorimetry (DSC) are used to develop well-defined structure–property correlations and to further clarify the contribution of Al_2O_3 as an element that improves thermal stability and network connectivity. Previous studies have mainly focused on complex/doped-glass systems where Al_2O_3 acts in conjunction with some other modifier or functional dopant. [12,13].

2. Materials and Methods

Three glass compositions were designed within the Li_2O–Al_2O_3–B_2O_3 system by keeping the B_2O_3 content fixed at 60 mol% and varying the Li_2O/Al_2O_3 ratio. The nominal molar compositions are summarized in Table 1. High-purity Li_2CO_3 (extra pure; Sigma-Aldrich, St. Louis, MO, USA), Al_2O_3 (99.73%; Sigma-Aldrich, St. Louis, MO, USA), and H_3BO_3 (99.5% AR; Sigma-Aldrich) were used without further purification and used as starting materials. The required amounts of each reagent were calculated on a molar basis, weighed to an accuracy of ±0.1 mg, and thoroughly mixed in an agate mortar until a homogeneous batch was obtained.

Table 1. Nominal compositions of the Li_2O–Al_2O_3–B_2O_3 glasses (mol%).

Glass ID	Al_2O_3 (mol%)	Li_2O (mol%)	B_2O_3 (mol%)
L1	10	30	60
L2	15	25	60
L3	20	20	60

Al_2O_3, aluminum oxide.

Each batch (≈30–40 g) was placed in a high-alumina crucible and preheated at 400–450 °C for 1 h to remove physically adsorbed water and to decarbonate the lithium carbonate. Because of their high purity alumina crucibles' excellent chemical inertness and thermal stability at the melting temperatures used for this research project, it was decided to use these types of crucibles to reduce possible contamination by material from the crucible itself. The melting conditions for all of the compositions of glass were the same (melting temperature and holding time); therefore, if there were any contributions from the crucible material to the differences in structure, physical properties, or thermal properties observed in the glass as the amount of Al_2O_3 increased, then these contributions would be negligible and would not have any influence on the calculations of glass composition or upon the overall findings of the research project. The crucible was then heated to 1100–1150 °C and held for 1.5–2 h, with occasional swirling of the melt to promote homogenization and bubble removal. The clear, bubble-free melt was poured onto a preheated stainless-steel plate and immediately pressed with another plate to form glass slabs with a thickness of about 2–3 mm. The as-quenched glasses were transferred to an annealing furnace and held at a temperature 20–30 °C below the glass transition temperature (T_g) for 1 h. This was followed by slow cooling (≈1–2 °C·min^{-1}) to room temperature to relieve internal stresses. A schematic representation of the melt–quenching steps is provided in Fig. 1. The resulting samples from the process are shown in Fig. 2.

Bulk density (ρ) of the prepared glasses was determined at room temperature using Archimedes' principle with distilled water as the immersion medium. Each density value was obtained as the average of at least three independent measurements for each glass composition, and the experimental uncertainty was within ±0.005 g·cm^{-3}. The molar volume (V_m) was calculated from the measured density and the molar mass (M) of each glass composition according to:

$$V_m = {}^{M}/_{\rho} \quad (1)$$

For XRD measurements, a portion of each glass sample was crushed and ground to a fine powder (particle size <75 μm). XRD patterns were recorded at room temperature using Cu Kα radiation over the 2θ range 10–70° with a step size of 0.02° on a Aeris Research Edition diffractometer (Malvern Panalytical, Almelo, Overijssel, Netherlands). The amorphous nature of the glasses was confirmed by the presence of broad diffuse halos and the absence of sharp Bragg peaks.

FTIR spectra were collected in the range 200–1700 cm^{-1} using the KBr pellet technique. Approximately 1 mg of finely ground glass powder was mixed with 100 mg of spectroscopic-grade KBr, ground again to ensure uniform dispersion, and then pressed into a transparent pellet under vacuum. All spectra were acquired on using an IRTracer-100 spectrometer (Shimadzu Corporation, Kyoto, Japan) within the range of 200–1700 cm^{-1} using the KBr pellet method at a resolution of 4 cm^{-1}, and at least 32 scans were averaged for each sample to improve the signal-to-noise ratio.

Differential scanning calorimetry was used to perform thermal analysis on using a METTLER TOLEDO DSC system with STAR software (Greifensee, Zurich, Switzerland) in a nitrogen flow environment. Approximately 20–25 mg of glass in powdered form was added to an alumina crucible and heated from room temperature to 700 °C at a constant heating rate of 10 °C·min^{-1}. The glass transition temperature (T_g) was defined by the start of the endothermic step, while the crystallization temperature (T_x) was defined by the start of the main exothermic peak. The thermal stability was then calculated as:

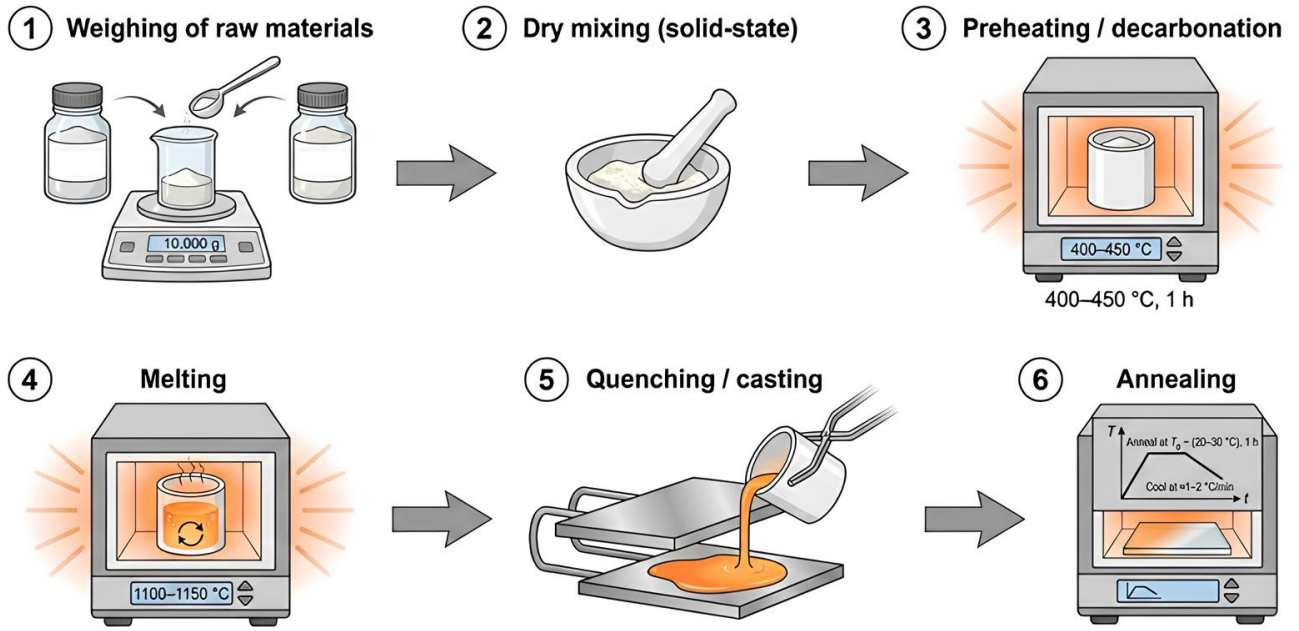

Fig. 1. Schematic illustration of the melt–quenching procedure used for preparing Li_2O–Al_2O_3–B_2O_3 glass samples, including solid-state (dry) mixing of the raw materials prior to melting.

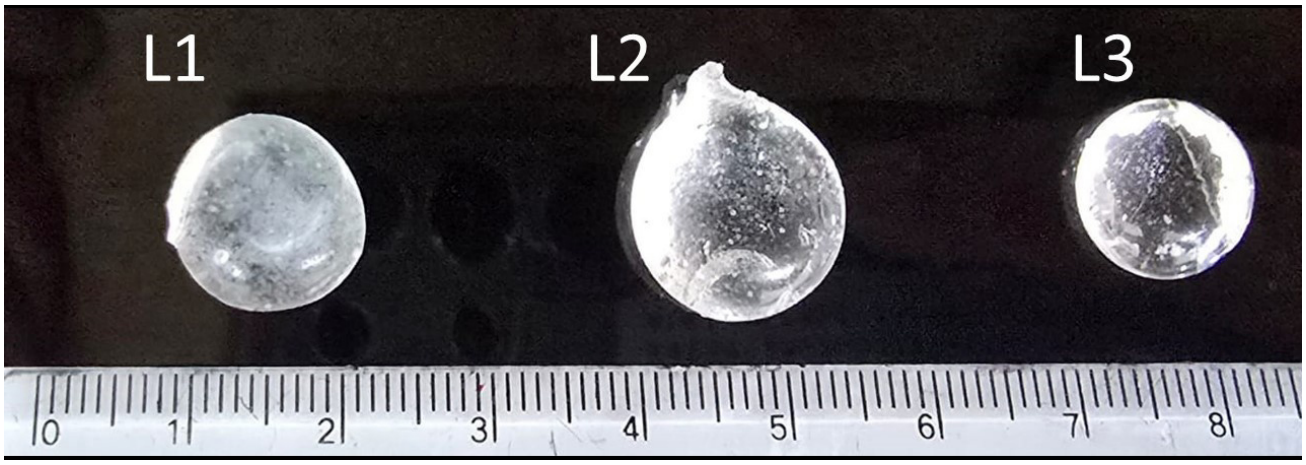

Fig. 2. Photographs of the prepared Li_2O–Al_2O_3–B_2O_3 glass samples. L1, L2, and L3 correspond to glass compositions containing 10, 15, and 20 mol% Al_2O_3, respectively, as listed in Table 1.

$$\Delta T = T_x - T_g \tag{2}$$

In this context, the thermal stability window ($\Delta T = T_x - T_g$) is a representation of the temperature interval that glass preserves the supercooled liquid state with no crystallization. Larger values of ΔT indicate higher resistance to devitrification during thermal processing. This reflects a glass network with higher structural rigidity and lower atomic mobility. For this reason, ΔT is a useful quantitative measure for the relative thermal stability between different glass compositions. The overall workflow of the characterization techniques used in this study is shown in Fig. 3.

Fig. 1 illustrates the glass preparation procedure, whereas Fig. 3 summarizes the sequence of characterization techniques applied to the prepared samples.

3. Results

Table 2 and Fig. 4 show the XRD analysis of the prepared glass samples L1, L2, and L3. All three spectra exhibited a single broad halo extending across $2\theta \approx 25$–$35°$, with no observable sharp reflections throughout the scanned range (10–70°). The lack of distinct Bragg peaks indicates that the compositions are completely amorphous. The information supports that there is a significant amount of structural disorder (i.e., no long-range order) of the glass network and that the glass network is made up

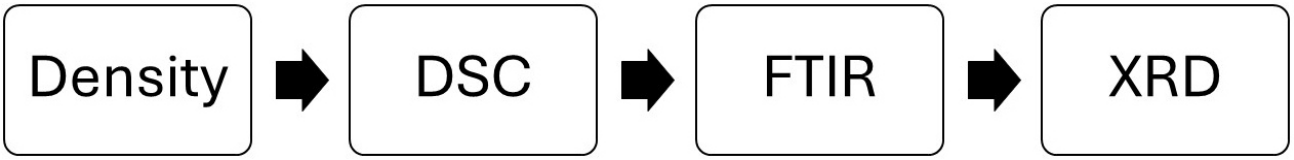

Fig. 3. Schematic representation of the characterization workflow used in this study. DSC, differential scanning calorimetry; FTIR, Fourier transform infrared spectroscopy; XRD, X-ray diffraction.

of a random mixture of BO_3 and BO_4 units, which create diffuse patterns. The gradual increase in Al_2O_3 concentration did not promote crystallinity in the resulting glass samples, since there were no measurable increases in peak height or any new structural characteristics within the XRD spectra due to the presence of Al in the glass network (intermediate-forming species or network-modifying species). The same trend was observed in lithium borate systems, which showed that incorporating Al_2O_3 will increase the structural rigidity of the glass structure while also maintaining its amorphous character [11].

Table 2. XRD halo parameters (center position and FWHM) for L1–L3 glasses.

Sample	Halo center (2θ)	FWHM (°)	Relative Intensity
L1	29.8°	21.5°	1.00
L2	30.5°	20.8°	1.12
L3	31.2°	20.1°	1.28

FWHM, full width at half maximum.

FTIR spectra of L1, L2 and L3 glass specimens were taken in the range of 200 cm^{-1} to 1700 cm^{-1} (Fig. 5). The spectra indicate the presence of characteristic vibrational modes characteristic of the borate glass network. The spectral region from 1200 cm^{-1} to 1550 cm^{-1} contains a broad feature that exhibits a noticeable baseline variation, which may contain noise and other artifacts. However, this region is largely attributed to an overlapping combination of vibrational contributions of the trigonal borate structural units [14,15]. Another major absorption band appears at approximately 1000 cm^{-1} to 1200 cm^{-1} due to the stretching vibrations of tetrahedral borate units [14,15]. The relative intensity of this band increases as the Al_2O_3 content increases and suggests that the glass network is becoming increasingly polymerized and interconnected.

The borate network bending vibrations are responsible for the absorption band between 800 cm^{-1} and 900 cm^{-1} [14,15] as a result of the increasing amount of Al_2O_3 in the glass mixture. The slight increase in the frequency of the band with higher amounts of Al_2O_3 indicates that the borate linkages formed within the glass structure are becoming more rigid and stronger. Another band in the absorption spectrum located at 550 cm^{-1} to 650 cm^{-1} is caused by the vibration of metal-oxygen bonds in the glass [14,15]. Features seen in the absorption spectrum below 400 cm^{-1} can be attributed to low-frequency lattice vibrations and bending modes due to heavier metal-oxygen linkages within the glass network. Although these modes are less sensitive to short-range structural changes, they can provide complementary information about the overall rigidity and connectivity of the glass matrix. The way this band behaves when additional Al_2O_3 is incorporated reinforces that aluminium has entered the glass network and has thus created a greater rigidity within the glass structure. The changes in spectra suggest that Al_2O_3 promotes the formation of a continuous structure in glass networks, increasing the number of structural links in the glass sample. This is also consistent with the patterns seen in density and thermal analysis of the three materials [14,15]. The FTIR band assignments and peak positions of the three glass samples are summarized in Table 3. For each of the three glass compositions, FTIR spectra were obtained at least twice under similar conditions to ensure consistency of the measurements. There were no noticeable differences in the spectrum between repeated measurements.

The measured (ρ) and estimated V_m can be summarized in Table 4. Density increased with increasing Al_2O_3 and molar volume decreased. This indicates that the network will have higher density as more open BO_3 groups are replaced by AlO_4 and BO_4 units. Although density increase and molar volume decrease indicate network compaction, a quantitative calculation of mean boron–boron separation distance would require detailed structural parameters (e.g., boron coordination fractions), which are beyond the scope of the present work. The measured values are L1 = 30.2 and for L2 = 29.5.

$$V_m = {}^{M}/_{\rho} \tag{3}$$

Here, M is the molar mass of the glass composition and ρ is the measured density.

The mean boron–boron separation distance was estimated from the measured molar volume using a number-density approximation (Table 5). The estimated mean boron–boron separation distance decreases with increasing Al_2O_3 content. This confirms the network compaction indicated by the density and molar volume measurements.

The decrease in molar volume with increased Al_2O_3 suggests a tighter packing of the network due to the sub-

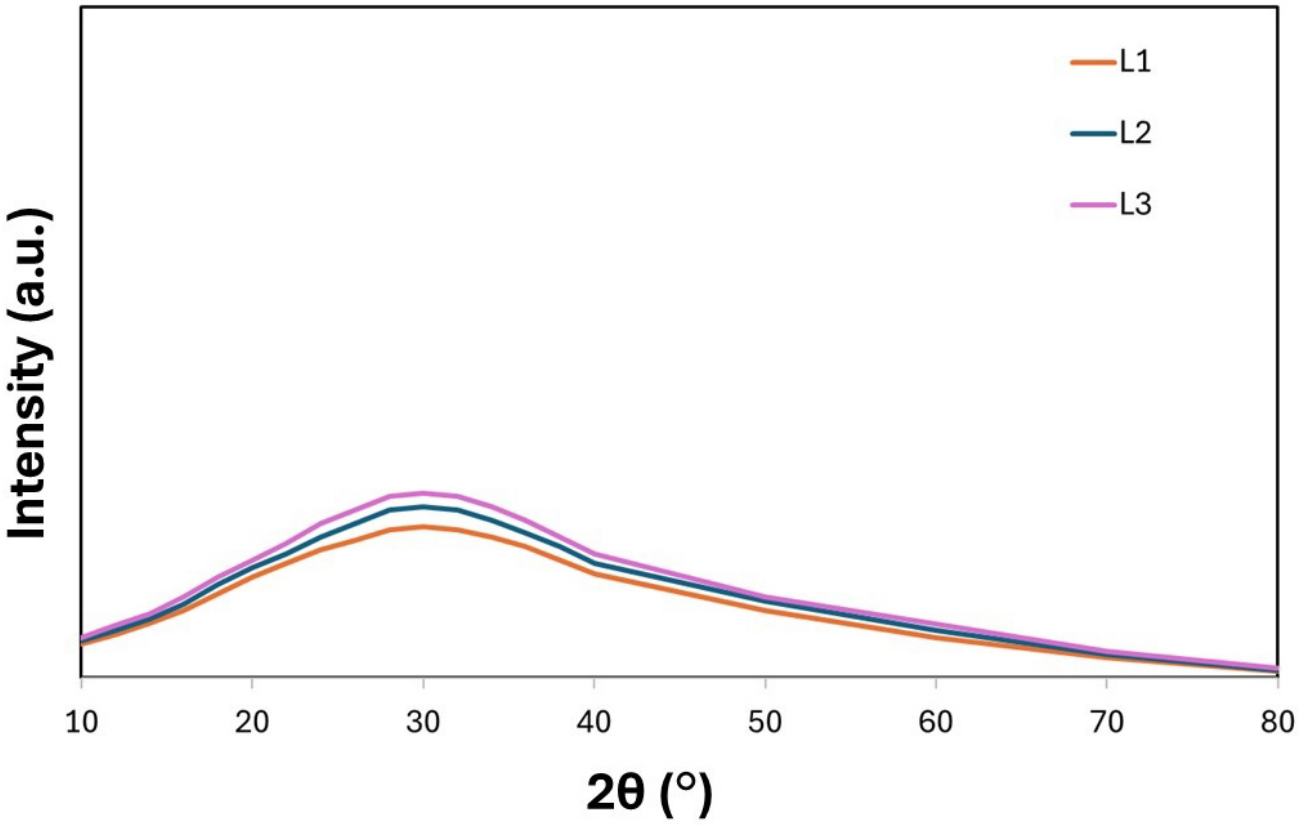

Fig. 4. XRD patterns of the L1, L2, and L3 glass samples. All diffractograms exhibit a broad amorphous halo centered around 2θ ≈ 25–35°, with no detectable crystalline peaks, confirming the fully amorphous nature of the prepared glasses.

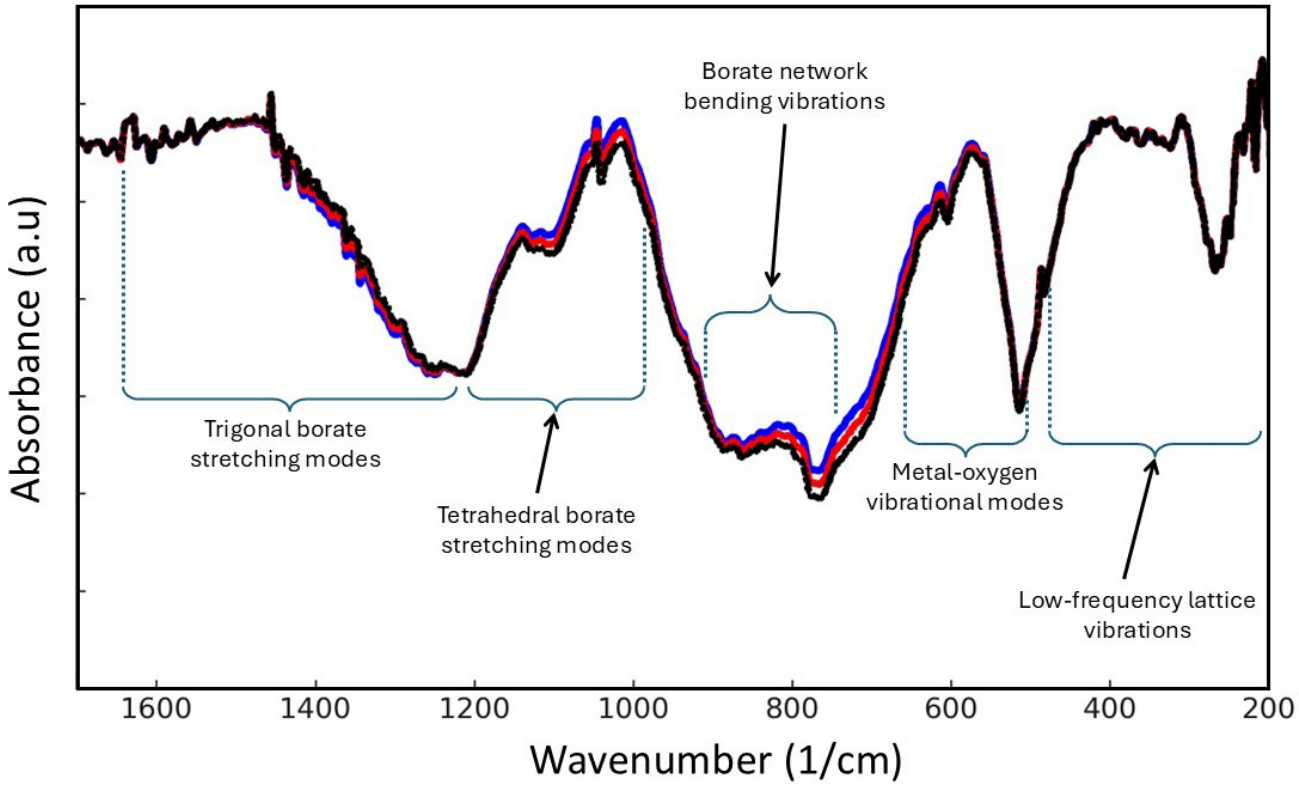

Fig. 5. FTIR spectra of L1, L2, and L3 lithium borate glass samples recorded in the range 200–1700 cm^{-1} .

Table 3. FTIR band assignments and peak positions for L1–L3 glasses.

L1 (cm^{-1})	L2 (cm^{-1})	L3 (cm^{-1})	Assignment (Vibrational mode)
1200–1550	1200–1550	1200–1550	Trigonal borate stretching modes
1000–1200	1000–1200	1000–1200	Tetrahedral borate stretching modes
800–900	800–900	800–900	Borate network bending vibrations
550–650	550–650	550–650	Metal–oxygen vibrational modes
<400	<400	<400	Low-frequency lattice vibrations

Table 4. Density and molar volume of L1–L3 glasses.

Glass ID	Density, ρ ($g \cdot cm^{-3}$)	Molar volume, V_m ($cm^3 \cdot mol^{-1}$)	Average molar mass ($g \cdot mol^{-1}$)
L1	2.02	30.2	60.93
L2	2.19	29.5	64.54
L3	2.37	28.7	68.14

V_m, molar volume.

Table 5. Estimated mean boron–boron separation distance ($d_{(B–B)}$) calculated from the measured molar volume.

Glass ID	Al_2O_3 (mol%)	V_m ($cm^3 \cdot mol^{-1}$)	N_B ($\times 10^{22}$ atoms$\cdot cm^{-3}$)	$d_{(B–B)}$ (Å)
L1	10	30.2	2.39	3.47
L2	15	29.5	2.45	3.443
L3	20	28.7	2.52	3.412

V_m, molar volume; N_B, the Boron atomic number density.

stitution of BO_3 by AlO_4. This requires charge compensation from Li^+—leading to a more rigid and denser structure [16,17,18]. The dependence of glass density on Al_2O_3 concentration is shown in Fig. 6.

The differential scanning calorimetry results are listed in Table 6. Both the T_g and T_x increase with increasing Al_2O_3 content. This behavior is typical for glasses with enhanced network connectivity and reduced non-bridging oxygen content.

Table 6. T_g, T_x, and thermal stability parameter (ΔT).

Glass ID	T_g (°C)	T_x (°C)	$\Delta T = T_x - T_g$ (°C)
L1	410	540	130
L2	425	560	135
L3	445	585	140

T_g, glass transition temperature; T_x, crystallization temperature.

A larger ΔT value indicates a reduced tendency of the glass to crystallize during heating. The gradual increase in ΔT from L1 to L3 suggests that Al_2O_3 addition enhances the rigidity of the glass network and improves its thermal resistance. This behavior is consistent with the FTIR results, which indicate an increase in tetrahedral structural units, and correlates with the observed decrease in molar volume [19,20,21]. The variation of T_g and T_x as a function of Al_2O_3 content is shown in Fig. 7.

The dependence of the thermal stability parameter (ΔT) on Al_2O_3 concentration is illustrated in Fig. 8.

4. Discussion

The synthesized glass of the L1–L3 series correspond to a specific structure-property relationship verified through the combined results of: XRD, FTIR and DSC. The XRD pattern established that all the samples were fully amorphous. Therefore, the evolution of the physical and thermal properties is solely due to the change in the network structure with increasing level of Al_2O_3 content and not introducing other crystallization phases. Furthermore, the FTIR spectra were used to identify the composition dependent vibrational bands of the BO_3; BO_4 and Al-O units. One can observe from the gradual emergence of the vibrational modes assigned to BO_4; as well as for the associated Al-O based vibrational mode, increasing concentrations of Al_2O_3 result in favoring the transition from three-coordinate B (BO_3) species to four-coordinate (or BO_4) species and the formation of tetrahedral AlO_4 units in the glass structure. The gradual increase in the number of four-coordinated BO_4 and tetrahedral AlO_4 units increase the rigidity and overall polymerization degree of the glass network, which leads to the denser glass structures as shown in Table 4.

The density increased from 2.02 to 2.37 $g \cdot cm^{-3}$, while the molar volume decreased from 30.2 to 28.7 $cm^3 \cdot mol^{-1}$. This demonstrates the formation of a higher density network, which contains fewer sites for open structures. It also indicates higher occurrences of tightly packed structure. The enhancement of the structure transition to be more connected corresponds to the charge-compensation process involving the stabilization of AlO_4 units by Li^+ in this system. This results a decrease in the amount of non-bridging

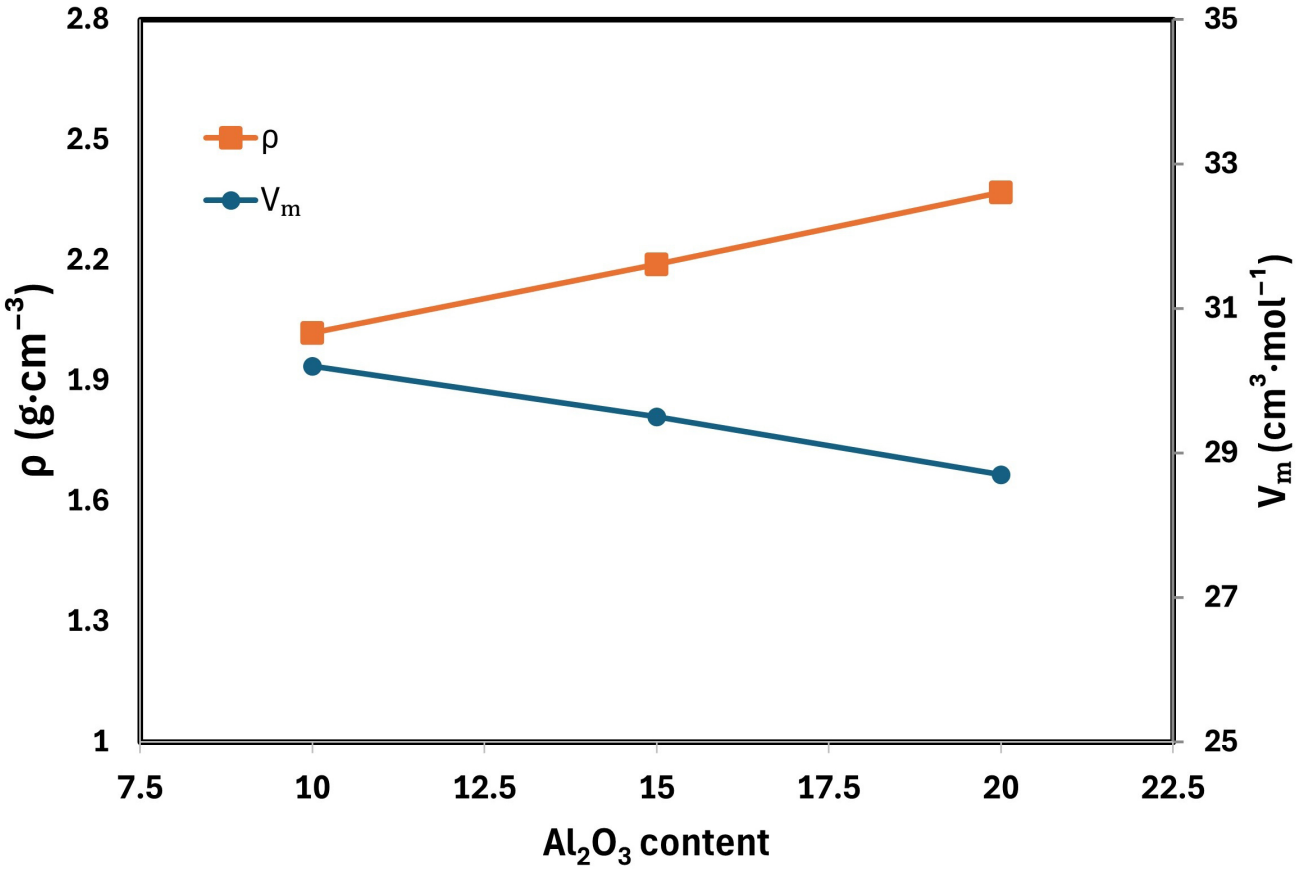

Fig. 6. Density and molar volume of Li_2O–Al_2O_3–B_2O_3 glasses as a function of Al_2O_3 content.

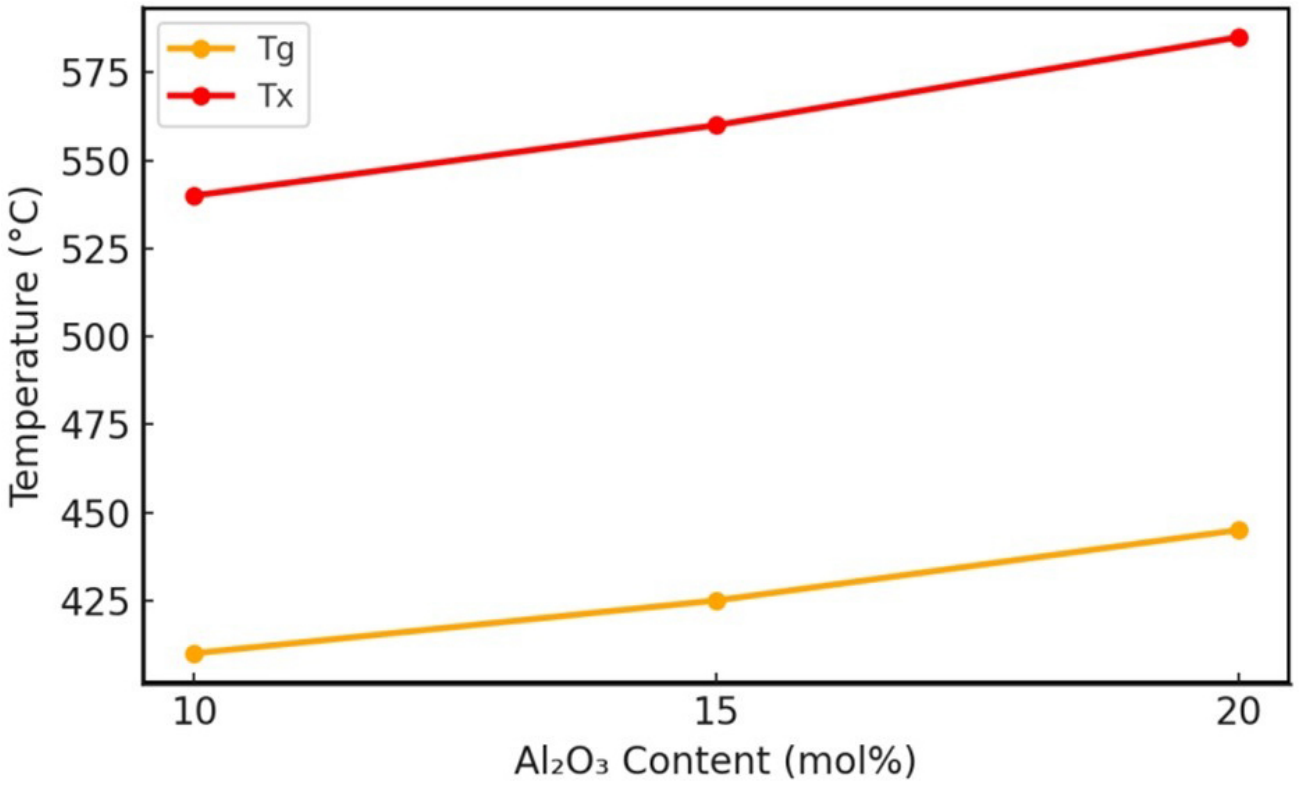

Fig. 7. Variation of glass transition temperature (T_g) and crystallization temperature (T_x) as a function of Al_2O_3 content.

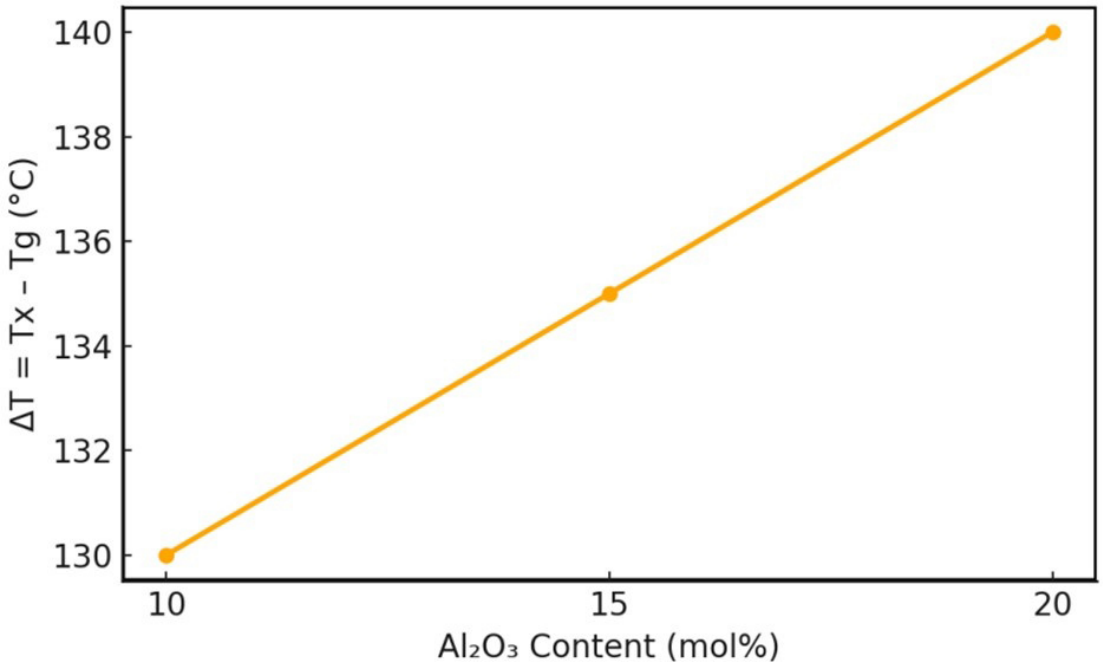

Fig. 8. Thermal stability parameter ($\Delta T = T_x - T_g$) of the glasses as a function of Al_2O_3 content.

oxygen (NBOs), while cross-linking becomes more favorable within the network. Structural hardening in alumina borate glasses was reported previously to be linked to their elevated temperatures durability [21,22,23,24].

This interpretation is also supported by the DSC results. T_g and T_x shift at higher temperature showing an augmentation in site-average bonding energy or network connectivity when Al_2O_3 is introduced. The increase of the thermal stability parameter ΔT (from 130 to 140 °C) indicates that these glasses become more resistant to crystallization upon heat treatment. This improved stability is due to the higher structural connectivity supplied by AlO_4 and BO_4, which hinders mobility that favors nucleation and growth of crystalline phases.

In general, the relationship between FTIR data, density/molar volume behavior and DSC parameters show that Al_2O_3 plays a role as network-forming oxide in Li_2O–Al_2O_3–B_2O_3 system. Its inclusion enhances the borate network, densifies structure and enhances thermal stability. These results confirm the beneficial role of Al_2O_3 in the construction of borate glasses for durable, controlled-dissolution glasses and devitrification resistant materials.

Limitations

This study examined the impact of Al_2O_3 for the composition range of 10–20 mol%. For this reason, the insights concluded from this study are limited to this compositional interval. No baseline sample (0 mol%) was not included in the reported results. The analysis provides a comparison between the samples mentioned above and does not extrapolate the observed trends to other compositions. Finally, the B-B separation was estimated from the V_m data.

5. Conclusions

Lithium borate glasses with 10–20 mol% of Al_2O_3 were prepared using the melt–quenching method in the present work. The structural and thermal behavior as well as spectroscopic study indicates that Al_2O_3 strongly enhances the strength and stability of the borate network. XRD data showed that all the samples were completely amorphous without any discernible crystalline phase. FTIR spectra indicated increased network polymerization from BO_3 to BO_4 with increasing Al_2O_3 content. A systematic increase in the measured density was observed for all Al-doped samples, while the calculated molar volume decreased, indicating improved structural compactness. The results of DSC analysis were consistent with the above interpretation, where an upward trend in T_g and T_x and higher thermal stability (ΔT) was observed. These collective results serve to confirm that Al_2O_3 is a strong network former in lithium borate glasses, contributing to the densification of glass structure, enhancement of polymerization degree and endow them with increased thermal stability. Such results reveal promising potentials of Al-substituted borate glasses as thermally and structurally stable glass networks for practical use.

Availability of Data and Materials

All datasets on which the conclusions of a manuscript depend are available to readers on request by email.

Author Contributions

MKA and AQT designed the research study. MKA performed the research. AQT analyzed the data. Both au-

thors contributed to critical revision of the manuscript for important intellectual content. Both authors read and approved the final manuscript. Both authors have participated sufficiently in the work and agreed to be accountable for all aspects of the work.

Ethics Approval and Consent to Participate

Not applicable.

Acknowledgment

The authors acknowledge the support and technical support given by Al-Karkh University of Science staff.

Funding

This research received no external funding.

Conflicts of Interest

The authors declare no conflicts of interest.

References

[1] Topper B, Möncke D. Structure and Properties of Borate Glasses. In Obata A, Brauer DS, Kasuga T (eds.) Phosphate and Borate Bioactive Glasses (pp. 162–191). The Royal Society of Chemistry: Croydon, UK. 2022.

[2] Brow R, Tallant DR. Structural design of sealing glasses. Journal of Non–Crystalline Solids. 1997; 222: 396–406. https://doi.org/10.1016/S0022–3093(97)90142–3

[3] Wright AC, Vedishcheva NM. Borate Networks: Rigidity versus Dimensionality. Physics and Chemistry of Glasses: European Journal of Glass Science and Technology Part B. 2016; 57: 1–14. https://doi.org/10.13036/17533562.57.1.087

[4] Dimitrov V, Komatsu T. Interionic Interactions, Electronic Polarizability and Optical Basicity of Oxide Glasses. Journal of the Ceramic Society of Japan. 2000; 108: 330–338. https://doi.org/10.2109/jcersj.108.1256_330

[5] Fernandes HR, Kapoor S, Patel Y, Ngai K, Levin K, Germanov Y, et al. Composition–structure–property relationships in Li2O–Al2O3–B2O3 glasses. Journal of Non–Crystalline Solids. 2018; 502: 142–151. https://doi.org/10.1016/j.jnoncrysol.2018.08.005

[6] El Hayek R, Ferey F, Florian P, Pisch A, Neuville DR. Structure and properties of lime alumino–borate glasses. Chemical Geology. 2017; 461: 75–81. https://doi.org/10.1016/j.chemgeo.2016.11.025

[7] Adamiv VT, Burak YV, Girnyk IS, Teslyuk IM. Thermal properties of alkaline and alkaline–earth borate glasses. Functional Materials. 2013; 20: 52–58.

[8] Othman H, Valiev D, Polisadova E. Structural and mechanical properties of zinc aluminoborate glasses with different content of aluminum oxide. Journal of Materials Science: Materials in Electronics. 2017; 28: 4647–4653. https://doi.org/10.1007/s10854–016–6103–z

[9] Morsy MA, Garrison TF, Kessler MR, Mhareb MHA, El-Deen HZ. Structural Elucidation of Lithium Borate Glasses Using XRD, FTIR, and EPR Spectroscopy. ACS Physical Chemistry Au. 2025; 5: 227–238. https://doi.org/10.1021/acsphyschemau.4c00106

[10] Klyuev VP and Pevzner BZ. The Influence of Aluminum Oxide on the Thermal Expansion, Glass Transition Temperature, and Viscosity of Lithium and Sodium Aluminoborate Glasses. Glass Physics and Chemistry. 2002; 28: 207–220. https://doi.org/10.1023/a:1019954010719

[11] Song L, Wang Y, Hannon AC, Feller S, Li W, Zhou Y, et al. Structural investigation of lithium borate glasses by Raman spectroscopy: Quantitative evaluation of structural units and its correlation with density. Journal of Non–Crystalline Solids. 2023; 616: 122478. https://doi.org/10.1016/j.jnoncrysol.2023.122478

[12] Welch RS, Astle S, Youngman RE, Mauro JC. High–coordinated alumina and oxygen triclusters in modified aluminosilicate glasses. International Journal of Applied Glass Science. 2022; 13: 388–401. https://doi.org/10.1111/ijag.16565

[13] Alomairy S, Aboraia AM, Shaaban ER, Shaaban KS. Comparative Studies on Spectroscopic and Crystallization Properties of Al2O3 –Li2O– B2O3–TiO2 Glasses. Brazilian Journal of Physics. 2021; 51: 1237–1248. https://doi.org/10.1007/s13538–021–00928–1

[14] Pontuschka WM, Kanashiro LS, Courrol LC. Luminescence Mechanisms for Borate Glasses: the Role of Local Structural Units. Glass Physics and Chemistry. 2001; 27: 37–47. https://doi.org/10.1023/A:1009507803955

[15] Möncke D, Kamitsos EI, Palles D, Limbach R, Winterstein-Beckmann A, Honma T, et al. Transition and post-transition metal ions in borate glasses: Borate ligand speciation, cluster formation, and their effect on glass transition and mechanical properties. The Journal of Chemical Physics. 2016; 145: 124501. https://doi.org/10.1063/1.4962323

[16] Osipov AA, Eremyashev VE, Mazur AS, Tolstoi PM, Osipova LM. Coordination state of aluminum and boron in barium aluminoborate glass. Glass Physics and Chemistry. 2016; 42: 230–237. https://doi.org/10.1134/s1087659616030111

[17] Boora M, Malik S, Kumar V, Bala M, Arora S, Rohilla S, et al. Investigation of structural and impedance spectroscopic properties of borate glasses with high Li+ concentration. Solid State Ionics. 2021; 368: 115704. https://doi.org/10.1016/j.ssi.2021.115704

[18] Ali AA, Rammah YS, El–Mallawany R, Souri D. FTIR and UV spectra of pentaternary borate glasses. Measurement. 2017; 105: 72–77. https://doi.org/10.1016/j.measurement.2017.04.010

[19] Ahmed MR, Ashok B, Ahmmad SK, Hameed A, Chary MN, Shareefuddin M. Infrared and Raman spectroscopic studies of Mn^{2+} ions doped in strontium alumino borate glasses: Describes the role of Al_2O_3. Spectrochimica Acta. Part A, Molecular and Biomolecular Spectroscopy. 2019; 210: 308–314. https://doi.org/10.1016/j.saa.2018.11.053

[20] Gautam C, Yadav AK, Singh AK. A Review on Infrared Spectroscopy of Borate Glasses with Effects of Different Additives. ISRN Ceramics. 2012; 2012: 1–17. https://doi.org/10.5402/2012/428497

[21] Saidu A, Wagiran H, Saeed MA, Alajerami YSM. Structural properties of Zinc Lithium borate glass. Optics and Spectroscopy. 2014; 117: 396–400. https://doi.org/10.1134/s0030400x14090239

[22] Mascaraque N, Januchta K, Frederiksen KF, Youngman RE, Bauchy M, Smedskjaer MM. Structural dependence of chemical durability in modified aluminoborate glasses. Journal of the American Ceramic Society. 2019; 102: 1157–1168. https://doi.org/10.1111/jace.15969

[23] Padmaja G, Kistaiah P. Infrared and Raman spectroscopic studies on alkali borate glasses: evidence of mixed alkali effect. The Journal of Physical Chemistry. a. 2009; 113: 2397–2404. https://doi.org/10.1021/jp809318e

[24] Siuzdak Weber KA., Shelby JE. Properties of lithium aluminoborate glasses. Physics and Chemistry of Glasses European Journal of Glass Science and Technology Part B. 2022; 63: 111–118. https://doi.org/10.13036/17533562.63.2.15